Correspondence to:
H. Kim,
hk1530@princeton.edu

Changes in the Climate System Dominate Inter-Annual Variability in Flooding Across the Globe

Hanbeen Kim[1,2] ![ORCID], Gabriele Villarini[1,2] ![ORCID], Conrad Wasko[3] ![ORCID], and Yves Tramblay[4] ![ORCID]

[1]High Meadows Environmental Institute, Princeton University, Princeton, NJ, USA, [2]Department of Civil and Environmental Engineering, Princeton University, Princeton, NJ, USA, [3]Department of Infrastructure Engineering, The University of Melbourne, Parkville, VIC, Australia, [4]Espace-Dev (University of Montpellier, IRD), Montpellier, France

Abstract Extreme flood events have regional differences in their generating mechanisms due to the complex interaction of different climate and catchment processes. This study aims to examine the capability of climate drivers to capture year-to-year variability in global flood extremes. Here, we use a statistical attribution approach to model seasonal and annual maximum daily discharge for 7,886 stations worldwide, using season- and basin-averaged precipitation and temperature as predictors. The results show robust performance of our seasonal climate-informed models in describing the inter-annual variability in seasonal and annual maximum discharges regardless of the geographical region, climate type, basin size, degree of regulation, and impervious area. The developed models enable the assessment of the sensitivity of flood discharge to precipitation and temperature changes, indicating their potential to reliably project changes in the magnitude of flood extremes.

Plain Language Summary Successfully modeling the changes in magnitudes of flood events is challenging due to the complexity of flood-driving processes, which vary depending on region and season. Here, we examine how seasonal precipitation and temperature can describe changes in the flood magnitudes. Although we only consider these basic climate factors as predictors, our climate-informed models consistently show a good performance in capturing the year-to-year variability in the magnitude of seasonal and annual flooding events across 7,886 stations worldwide. These results show the suitability of seasonal precipitation and temperature as proxies for different climate and catchment processes leading to flooding.

1. Introduction

In the last two decades, flooding affected 1.6 billion people globally and incurred $651 billion in economic costs, the highest and the second highest of any other environmental hazards, respectively (CRED & UNDRR, 2020). As warming trends are globally expected to continue over the 21st century, flood damages are expected to increase in the future (e.g., Alfieri et al., 2017; IPCC, 2021) in light of climatic and socio-economic changes (Merz et al., 2021; Wasko, Sharma, & Pui, 2021). Therefore, addressing questions about changes in flooding has important socio-economic consequences for our adaptation and mitigation strategies.

The detection of trends in flood extremes has received much attention in hydrology. However, it remains a challenge to achieve consensus on the detection of changes because of its lack of evidence (e.g., Archfield et al., 2016), sensitivity to data length (e.g., Do et al., 2017), and strong variations by basin alteration (e.g., Hodgkins et al., 2019), climate region (e.g., Slater et al., 2021), and catchment size (e.g., Bertola et al., 2020). Furthermore, extrapolating flood extremes directly from these findings for future projection is not reliable because the historical trends might not be representative of future conditions, especially if we do not understand the physical processes responsible for these changes (e.g., Do et al., 2020; Kim & Villarini, 2024; Mallakpour et al., 2018; Schlef et al., 2018; Villarini & Wasko, 2021; S. Zhang, Zhou, et al., 2022).

With this background, there is a growing interest in the attribution of changes in flood extremes based on understanding the driving flood processes (e.g., Alifu et al., 2022; Kim & Villarini, 2023a; Merz et al., 2022; Prosdocimi et al., 2015). Flood generating mechanisms vary geographically and seasonally depending on the climate drivers (e.g., summer monsoon, snowmelt, rain-on-snow, tropical cyclone). Together with various physical processes, antecedent soil moisture is an important factor in flood generation worldwide (e.g., Berghuijs et al., 2019; Stein et al., 2021; Tramblay et al., 2022; Wasko et al., 2020a). As such, climate variability and its feedbacks with the land surface play a significant role in determining flood mechanisms. Furthermore, climate

variability can affect changes in flood magnitude not only by itself (Liu et al., 2022), but also by shifting flood-generating processes (Jiang et al., 2022; Kemter et al., 2020; Tarasova et al., 2023).

This study aims to examine how climate drivers can describe changes in the magnitude of flood extremes worldwide. Despite the complexity of the flood generating mechanisms, Kim and Villarini (2023a) showed that seasonal precipitation and temperature are the key predictors as proxies for different physical processes to describe the changes in flood extremes across the conterminous United States (U.S.). Here we extend the statistical attribution framework developed by Kim and Villarini (2023a) to the global scale and assess how well the seasonal climate predictors describe seasonal and annual maximum daily discharges worldwide.

2. Data

2.1. Streamflow Databases

We use four data sources providing streamflow observations and their basin boundaries: (a) Global Streamflow Indices and Metadata archive (GSIM) (Do et al., 2018a; Gudmundsson et al., 2018a); (b) African Database of Hydrometric Indices (ADHI) (Tramblay et al., 2021); (c) Australian Bureau of Meteorology's Hydrologic Reference Stations (HRS); and (d) U.S. Geological Survey (USGS). The GSIM is a global collection of metadata and indices derived from daily streamflow time series observed between 1806 and 2016 at more than 35,000 streamgages from 12 databases (Do et al., 2018a). It provides quality-controlled indices including mean, maximum, and minimum daily streamflows for monthly, seasonal, and yearly temporal scales (Gudmundsson et al., 2018a). The ADHI is an African database of indices computed from quality-controlled daily discharges at 1,466 stations over the period 1950–2018, including monthly time series of mean, maximum, and minimum daily discharges. The HRS provides a high-quality, unimpacted, daily streamflow series observed to early 2019 at 467 stations across Australia. The USGS also provides daily streamflow series over the U.S. and its territories.

From the above-mentioned data sources, we obtain the seasonal maximum mean daily discharge series between 1949 and 2019 and screen the stations as follows.

1. Only seasonal maxima based on at least 85 daily observations are considered (Gudmundsson et al., 2018a).
2. Only years with seasonal maxima for all four seasons are considered. Here we consider the water year that starts in the season with the lowest median of seasonal maxima among the four seasons, similar to Wasko et al. (2020b).
3. Only stations for which four seasonal maxima are available for at least 30 years are considered.

Additionally, we excluded the stations whose basin is located within a "polar" region based on the Köppen-Geiger climate classification (Beck et al., 2018). Although GSIM provides observations from streamgages worldwide, we use ADHI and HRS data sets for Africa and Australia, respectively, since they have more up-to-date observations with higher quality compared to GSIM. For the conterminous U.S., we use the USGS seasonal maximum discharges up to 2019 from Kim and Villarini (2023a). As a result, a total of 8,211 stations are selected (as mentioned below, this number is further reduced based on the modeling results). Figure S1 in Supporting Information S1 illustrates locations, basin boundaries, basin sizes, and record lengths of the selected stations worldwide, divided into seven regions (North America, NA; South America, SA; Europe, EU; Africa, AF; Northern Asia, NAS; Southern Asia, SAS; and Oceania, OC).

2.2. Meteorological Data

We consider gauge-based global precipitation and temperature data for modeling flood extremes. The Global Precipitation Climatology Center (GPCC) provides the Full Data Product (V2020) of gridded ($0.25° \times 0.25°$) monthly precipitations from 1891 to 2019 by interpolating 85,000+ rainfall gauges worldwide (Becker et al., 2013; Schneider et al., 2020). From the GPCC V2020, we obtain monthly precipitation data. For temperature, we use the GHCN_CAMS gridded ($0.5° \times 0.5°$) 2 m temperature data set (Fan & Van Den Dool, 2008), a global monthly mean land surface air temperature from 1948 to present. We calculate basin-averaged values of monthly precipitation and temperature by taking the mean of the grid cells belonging to the basin area, and then compute the seasonal means of these basin-averaged monthly series (hereafter referred to as basin- and season-averaged precipitation and temperature).

3. Method

To model the inter-annual variability in flood extremes, we apply the statistical attribution approach developed by Kim and Villarini (2023a). For each streamgage and each season, we first develop a statistical model for seasonal maximum mean daily discharge using climate predictors (DJF: December-February; MAM: March-May; JJA: June-August; SON: September-November). For this, we use the nonstationary gamma distribution (or zero-adjusted gamma distribution for observations with zero discharge values), widely used for modeling extreme flood magnitude (e.g., Kim & Villarini, 2023a, 2023b; Miniussi et al., 2020). To attribute the inter-annual variability in seasonal maxima, basin- and season-averaged precipitation and temperature in the season of interest are used as covariates for the distribution parameters. We also consider the season prior to the season of interest to capture lagged effects (e.g., antecedent wetness). Based on the parameterization in the Generalized Additive Models for Location, Scale, and Shape (Rigby & Stasinopoulos, 2005), we can define location (μ), scale (σ), and the probability of zero discharge occurrence (ν) parameters of the gamma and zero-adjusted gamma distribution as below:

$$\log(\mu) = \mu_0 + \mu_1 P_{\text{con}} + \mu_2 T_{\text{con}} + \mu_3 P_{\text{lag}} + \mu_4 T_{\text{lag}} \tag{1}$$

$$\log(\sigma) = \sigma_0 + \sigma_1 P_{\text{con}} + \sigma_2 T_{\text{con}} + \sigma_3 P_{\text{lag}} + \sigma_4 T_{\text{lag}} \tag{2}$$

$$\log\left(\frac{\nu}{1-\nu}\right) = \nu_0 + \nu_1 P_{\text{con}} + \nu_2 T_{\text{con}} \tag{3}$$

where P_{con} (T_{con}) and P_{lag} (T_{lag}) are basin- and season-averaged precipitation (temperature) in the concurrent and previous seasons, respectively. Depending on the linear combination of predictors, we fit all possible models to the observed seasonal maximum discharge series for the whole period. We then select the best one based on the Schwarz's Bayesian criterion (Schwarz, 1978). If the distribution parameters are not estimated due to no convergence of the fitting procedure (i.e., maximum likelihood estimation) or the maximum value of $\hat{\mu}$ during the observation period is more than 10 times the observed highest seasonal maximum discharge, we consider the modeling not successful.

After selecting the best model for each season and station, we employ a Monte Carlo approach to simulate annual maximum daily discharge series by combining four seasonal models. Since the driest and wettest seasons are different geographically worldwide (Figures S2 and S3 in Supporting Information S1), we consider the water year whose beginning season is the season with the lowest median of seasonal maxima. For every year, we first generate one seasonal maxima from each of the four selected seasonal models and select the largest one as the annual maximum value. By iterating this step 1,000 times, we obtain the distribution of annual maximum daily discharge series over the whole observation years (see Kim & Villarini, 2023a for details). To assess the model performance in describing the inter-annual variability of flood extremes, we calculate the Spearman correlation coefficient between observations and the median (i.e., 50th percentile) of the modeled seasonal and annual maximum discharges. Furthermore, we conduct leave-one-out cross-validation to evaluate the model performance. For each season, we estimate the parameters of the best model excluding one seasonal maximum value at the time and predict its value based on the values of the predictors for the given year. We iterate this process for each year to obtain a time series of seasonal and annual maxima for the period of record. We then compute the Spearman correlation coefficient between the cross-validated time series and observations.

Finally, we perform sensitivity analyses to examine how the changes in seasonal climate predictors affect the changes in the magnitude of flood extremes. This data-driven approach is relevant to assess flood elasticity to climate drivers (Y. Zhang et al., 2023). We set changing conditions, adding climate drivers one by one, starting with the most important one. Because the tendency of temperature change is generally similar throughout seasons, we consider both T_{con} and T_{lag} changes at once. Consequently, we set three conditions for changing climate drivers: (a) only P_{con} changes (Con1); (b) both P_{con} and P_{lag} change (Con2); and (c) all four climate drivers change (Con3). Considering the range of projected changes in globally averaged annual land precipitation (Lee et al., 2021), we limit the change in precipitation to 10%, and do the same for temperature. We conduct Monte Carlo experiments by varying the climate predictors between −10% and 10% for each condition and season, allowing us to explore the sensitivity of the annual maximum discharges to changes in the drivers. Here we repeat the simulations 10,000 times to obtain more reliable flood quantiles with a lower annual exceedance probability
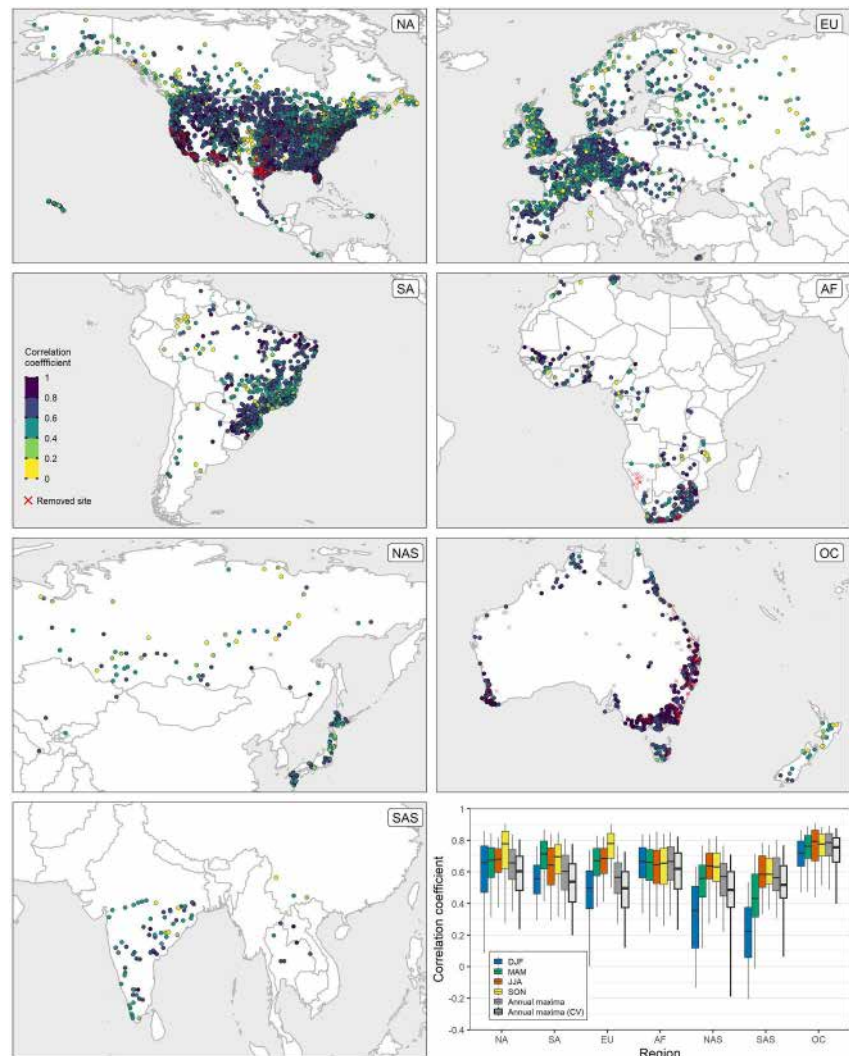
Figure 1. Maps and boxplots (dark gray) showing the model performance in simulating annual maximum discharge for 7,886 stations classified into seven regions. Red crosses represent the 325 stations removed due to the failure of the seasonal models. The boxplots also show the correlation coefficient based on leave-one-out cross-validation (light gray boxes) and seasonal models for DJF (blue boxes), MAM (green boxes), JJA (orange boxes), and SON (yellow boxes). In the boxplot, the limits of the box (whiskers) represent the 25th and 75th (5th and 95th) percentiles, while the line inside of the box indicates the median.

(AEP). For a given AEP (e.g., the 0.01-AEP refers to the 0.99 quantile), we obtain the median of the flood quantiles over all the observation years ($Q_{\mathrm{med}}^{\mathrm{AEP}}$); we then calculate its relative changes ($r\Delta Q_{\mathrm{med}}^{\mathrm{AEP}}$) based on the $Q_{\mathrm{med}}^{\mathrm{AEP}}$ with no changing condition ($Q.nc_{\mathrm{med}}^{\mathrm{AEP}}$) as below.

$$r\Delta Q_{\mathrm{med}}^{\mathrm{AEP}} = \frac{Q_{\mathrm{med}}^{\mathrm{AEP}} - Q.nc_{\mathrm{med}}^{\mathrm{AEP}}}{Q.nc_{\mathrm{med}}^{\mathrm{AEP}}} \times 100\ (\%) \tag{4}$$

4. Results and Discussion

Out of 8,211 stations, we evaluate the model performance for 7,886 stations with no model failure in all seasons. Our statistical approach performs well in reproducing the inter-annual variability of annual maximum discharges worldwide, having a correlation coefficient larger than 0.56 for half of the stations for all seven regions (Figure 1). OC shows the best performance, with 75% of the stations having a correlation coefficient larger than 0.7, followed by AF and NA, with the median correlation coefficient of 0.67 and 0.66, respectively. For the performance of the
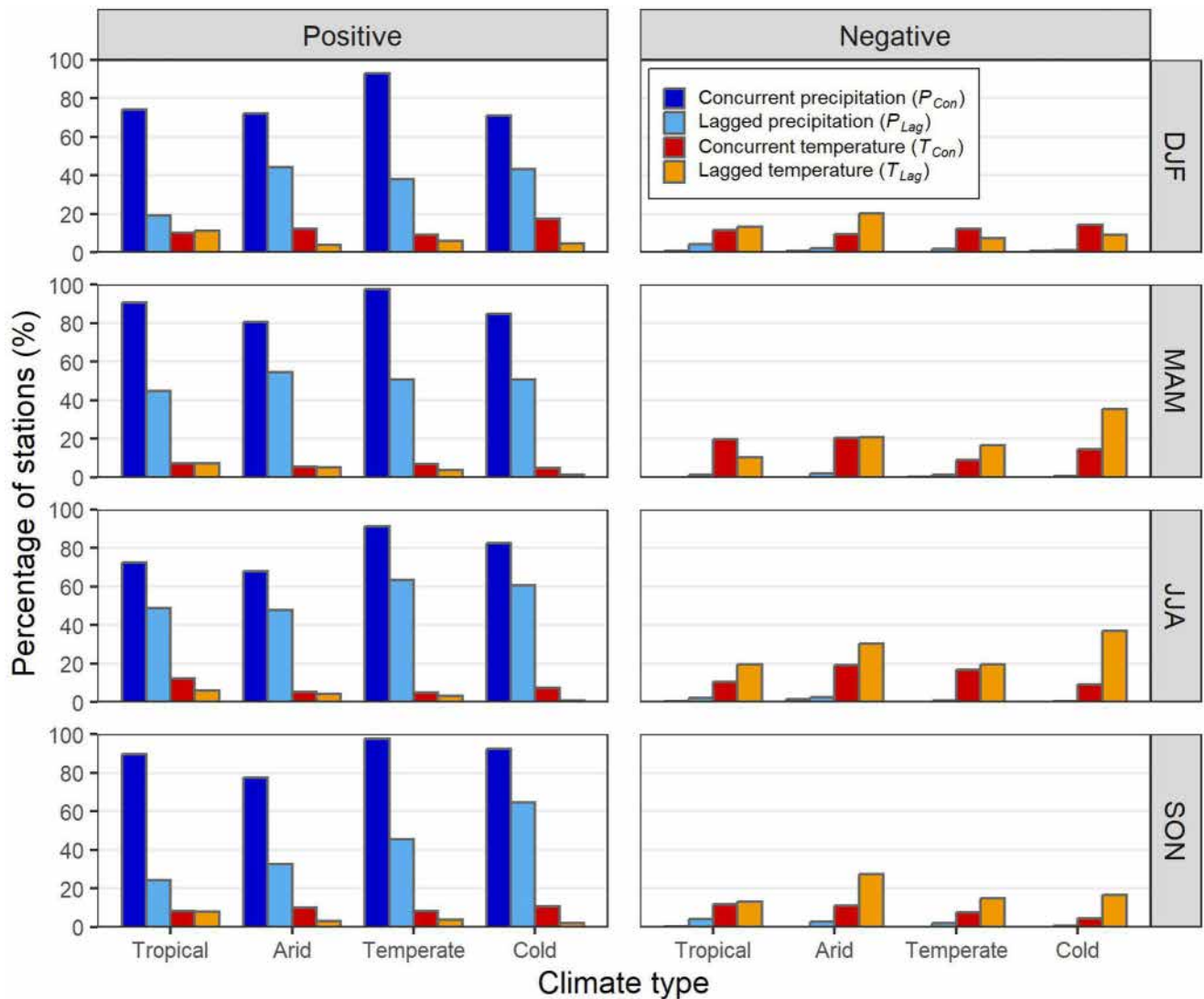
Figure 2. Covariate selection ratio of location parameter (μ) of the seasonal models depending on four climate types.

seasonal maxima, there are differences across the regions (colored boxplots in Figure 1). While OC and AF show similar performances regardless of season, NAS and SAS show limited performances especially in the DJF season, with the median correlation coefficients of 0.36 and 0.23, respectively. Given that the DJF season is the driest season for most stations in these regions (Figure S2 in Supporting Information S1; e.g., Yao et al., 2010), we want to examine if the climatic conditions of the basins affect the model performance. To do this, we stratify the results depending on four climate types (Tropical, Arid, Temperate, and Cold) (Figure S4 in Supporting Information S1). Although the DJF season shows the lowest performance among the four seasons regardless of climate type, our seasonal models generally perform well, with a median correlation coefficient larger than 0.53 for all climate types and seasons. This good seasonal performance leads to a good performance in simulating annual maxima, with 75% of the stations having a correlation coefficient larger than 0.5 for all climate types. Cross-validated annual maxima also exhibit good skills, with median correlation coefficients in the range of 0.49–0.76 and 0.54–0.61 depending on regions and climate types, respectively (light gray boxes in Figure 1 and Figure S4 in Supporting Information S1). These results indicate the robustness of our statistical approach in capturing the year-to-year variability of annual maximum discharges regardless of climate types.

To identify what climate drivers are responsible for the changes in the magnitude of seasonal maximum discharges, we investigate the selected covariates for the location parameter of each seasonal model. Figure 2 shows

the percentage of stations where the climate covariates are selected for the location parameter depending on climate type and season. P_{con} is the most selected covariate with a positive coefficient at more than 67% of stations for all seasons and climate types, indicating that seasonal precipitation in the concurrent season of interest is without doubt the most important climate driver for flood extremes. P_{con} is followed by P_{lag}, which is selected consistently worldwide with a positive coefficient. On the other hand, temperature is selected less often and shows a different pattern across the globe compared to precipitation. T_{lag} is generally selected at more stations than T_{con} and has a negative coefficient. Given that precipitation and temperature clearly have positive and negative relationships with soil moisture, respectively, the selection of P_{lag} and T_{lag} highlights their significant role in flood generation as proxies of antecedent wetness; T_{lag} is more frequently selected in the MAM and JJA seasons. These results point to the role of lagged climate predictors as a proxy for snow accumulation and melt in the snowmelt-dominated basins such as the northern U.S. (Welty & Zeng, 2021) and Europe (Berghuijs et al., 2019). NAS and SAS present the lowest covariate selection ratio in the DJF season (Figure S5 in Supporting Information S1), with no covariate selected for the location parameter at more than 30% of stations. In other words, at many of the stations, the best DJF model has a time-invariant location parameter, resulting in the poor performance of the model for this season in describing the year-to-year variability in flood magnitudes. The lack of covariate selection for the location parameter may be due to the limited suitability of our selected climate predictors in explaining the physical processes responsible for flood extremes in DJF in these regions. Nevertheless, given that the DJF season rarely contributes to the annual maxima in NAS and SAS (Figure S6 in Supporting Information S1), the limited performance of the DJF models does not impact the overall modeling of the annual maxima, which is the focus of this study.

We further examine if there is any difference in the climate covariate selection between concurrent and lagged seasons depending on basin-averaged aridity calculated from the Global Aridity Index and Potential Evapotranspiration Database—Version 3 (Global-AI_PET v3) (Zomer et al., 2022). Figure S7 in Supporting Information S1 shows the total covariate selection ratio of the location parameter for the four seasonal models depending on the four aridity classifications (UNEP, 1997). P_{con} is selected at 79.4% of the stations in the arid regions, and from 76.5% to 90.3% as the basins become wetter (i.e., from semi-arid to humid). On the other hand, P_{lag} is selected only at 31.3% of stations in the arid region, which is only slightly more than half as many as in the other aridity classes. Compared to precipitation, temperature does not exhibit a strong dependence on aridity. Only in the arid region, however, T_{con} is selected more often than T_{lag}. These results indicate that the drier the region, the smaller the influence of the lagged effects of precipitation and temperature (e.g., antecedent wetness) compared to their concurrent ones.

The flood response to climate drivers can be affected by physical characteristics of a river basin such as topographic (Edokpa et al., 2022) and anthropogenic (Konrad, 2016) factors closely related to rainfall-runoff processes (e.g., time of concentration, soil infiltration). Therefore, we examine how the performance of our climate-informed models is affected by the basins' physical characteristics. Here we consider the basin size, dam density, and average depth of dam capacity (i.e., dam storage capacity/basin size) available from the streamflow databases we considered (Figures S1 and S8 in Supporting Information S1). We also consider the ratio of impervious areas from the global impervious-surface data set (GISD30) (X. Zhang, Liu, et al., 2022). When we stratify the results depending on these four characteristics (Figure 3), it is difficult to find any clear pattern, suggesting that the climate drivers we considered have a greater influence on the inter-annual variability in the magnitude of flood extremes compared to the effect of basin size, dam density, average depth of dam capacity, and impervious area.

The above-mentioned results demonstrate the robustness of our statistical models across geographical regions, climate types, and basins' physical characteristics. Based on these models, we examine the sensitivity of flood extremes to changes in the climate drivers. Figure 4 shows the relative changes in the median of the 0.01-AEP discharge ($r\Delta Q_{med}^{0.01}$) for changes of -10%, -5%, $+5\%$, and $+10\%$ in the seasonal climate drivers, stratified by climate types. When only P_{con} changes (Con1), the $Q_{med}^{0.01}$ values change in the same direction, with ~95% of stations showing changing ratios smaller than those in P_{con} for all seasons and climate types. Con2 (i.e., both P_{con} and P_{lag} change) shows larger changes than for Con1, even though they are generally below the percentage change used for the sensitivity. The $r\Delta Q_{med}^{0.01}$ under these two conditions result from the selection of P_{con} and P_{lag} at most stations with a positive coefficient (Figure 2). When changing all four climate drivers (Con3), the overall patterns (i.e., median of boxplots) are similar to those under Con2, but there is much more variability among stations (orange boxes in Figure 4). To understand these results, we need to remember that T_{con} and T_{lag} can affect the
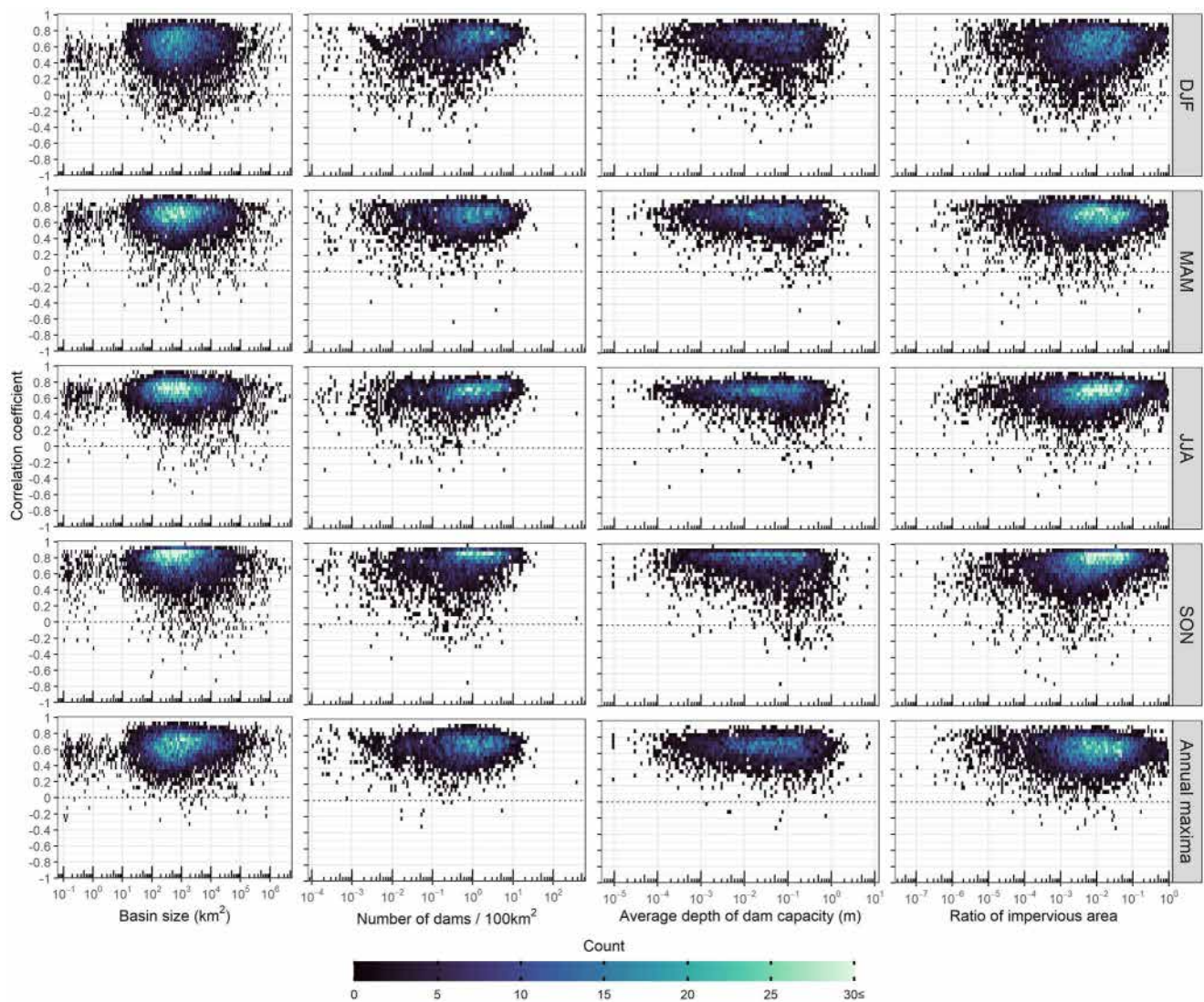
Figure 3. 2D histogram of the Spearman correlation coefficients calculated between observations and the median of the fitted and simulated distributions of seasonal (top-four rows) and annual maxima (bottom row), respectively, as a function of the basin size (first column), dam density (second column), average depth of dam capacity (third column), and ratio of impervious area (last column). Based on data availability, the results for dam density include stations belonging to the Global Streamflow Indices and Metadata (GSIM), African Database of Hydrometric Indices, and U.S. Geological Survey (USGS) databases, while those for average depth of dam capacity only to the GSIM and USGS ones.

changes in flood extremes both positively and negatively, causing either a compounding or offsetting effect of the precipitation changes. When we stratify the results depending on the seven regions, there are much more regional and seasonal differences in the distribution of $r\Delta Q_{\mathrm{med}}^{0.01}$ (Figure S9 in Supporting Information S1), suggesting that temperature changes may modulate the effect of precipitation on flood extremes by modulating seasonally and locally different flood generation processes (e.g., moisture-holding capacity, antecedent conditions, snowmelt). This sensitivity analysis allows not only the identification of the key seasons controlling the changes in flood extremes, but also understanding the potential response of annual flood peaks to changes in seasonal precipitation and temperature.

5. Conclusions

We investigated how well season- and basin-averaged precipitation and temperature can explain the inter-annual changes in the magnitude of flood extremes at 7,886 basins worldwide. Despite using at most only four predictors averaged across the entire season and basin, our models showed robust performance in capturing year-to-year
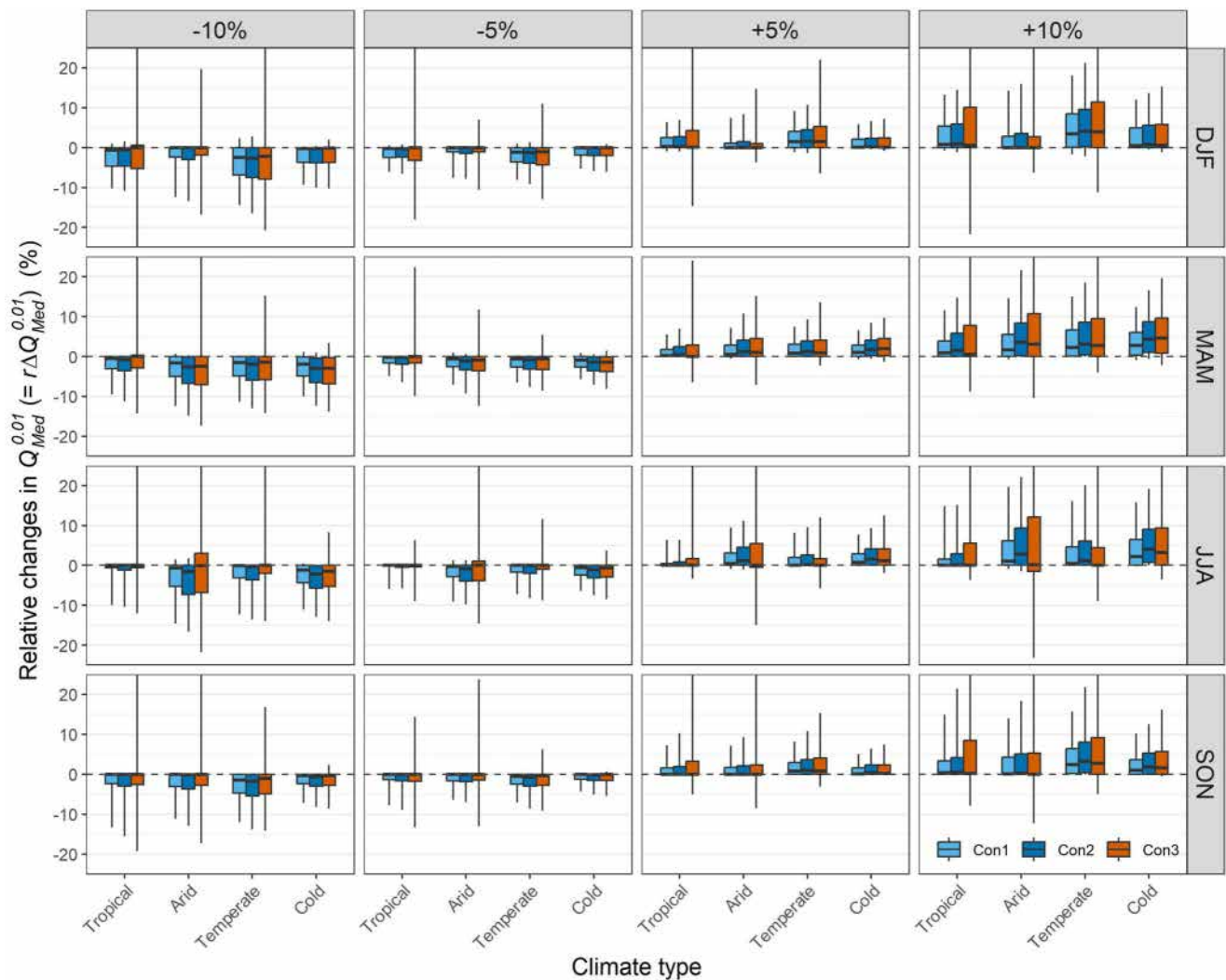
Figure 4. Sensitivity of the median of 0.01-annual exceedance probability discharge ($Q_{med}^{0.01}$) to changes in only concurrent precipitation (Con1; light blue boxes), both concurrent and lagged precipitations (Con2; blue boxes), and all four climate drivers (Con3; orange boxes) depending on climate types. Each column shows the results for four different changes (-10%, -5%, $+5\%$, and $+10\%$) in climate drivers, while each season's results are presented in a row.

variability in seasonal and annual maximum daily discharges regardless of the geographical region, climate type, basin size, and dam density. These results suggest that seasonal precipitation and temperature are suitable to characterize the complex interplays of different climate and catchment processes leading to peak discharges. The suitability of seasonal precipitation is consistent with Liu et al. (2022), who showed that precipitation with longer durations (e.g., 30 and 90 days) dominates the changes in global flood magnitude, while precipitation with shorter durations (e.g., 1 and 7 days) has more limited impacts.

In addition to the robustness of our climate-informed models, they enabled a sensitivity analysis of flood extremes to changes in precipitation and temperature. Based on our results, we should not expect that a certain percentage of changes in seasonal precipitation would lead to the same magnitude changes in annual maximum discharge, notably due to the strong influence of soil moisture storage in many regions (Wasko, Nathan, et al., 2021) and the change/differing of dominant flooding mechanisms (Quintero et al., 2022; S. Zhang, Zhou, et al., 2022). Although this study considered only 12 scenarios (i.e., 3 conditions × 4 changing rates) of changing climate drivers, these nonlinearities in the system can be further assessed by considering more combinations and changing rates of climate drivers. Another advantage of this modeling framework is that we do not assume a fixed seasonal contribution to the annual maximum discharge; instead, the mixing varies from year to year to reflect the intra-annual variability in precipitation and temperature.

Finally, given that precipitation and temperature are commonly available from numerous global climate models, we expect that our models can enable to reliably project changes in flood extremes as well as in their generating processes.

Data Availability Statement

The catchment boundary and time series indices of GSIM dataset can be found in Do et al. (2018b) and Gudmundsson et al. (2018b), respectively. The ADHI dataset is available in Tramblay and Rouché (2020). The dataset of HRS can be accessed from the Bureau of Meteorology website: http://www.bom.gov.au/water/hrs/. GPCC V2020 and GHCN_CAMS are publicly available through the NOAA Physical Sciences Laboratory websites: https://psl.noaa.gov/data/gridded/data.gpcc.html and https://psl.noaa.gov/data/gridded/data.ghcncams.html, respectively. The Global-AI_PET_v3 dataset is available in Trabucco and Zomer (2019). The GISD30 dataset can be found in Liu et al. (2021).

References

Alfieri, L., Bisselink, B., Dottori, F., Naumann, G., de Roo, A., Salamon, P., et al. (2017). Global projections of river flood risk in a warmer world. *Earth's Future*, *5*(2), 171–182. https://doi.org/10.1002/2016EF000485

Alifu, H., Hirabayashi, Y., Imada, Y., & Shiogama, H. (2022). Enhancement of river flooding due to global warming. *Scientific Reports*, *12*(1), 20687. https://doi.org/10.1038/s41598-022-25182-6

Archfield, S. A., Hirsch, R. M., Viglione, A., & Blöschl, G. (2016). Fragmented patterns of flood change across the United States. *Geophysical Research Letters*, *43*(19), 10232–10239. https://doi.org/10.1002/2016GL070590

Beck, H. E., Zimmermann, N. E., McVicar, T. R., Vergopolan, N., Berg, A., & Wood, E. F. (2018). Present and future Köppen-Geiger climate classification maps at 1-km resolution. *Scientific Data*, *5*(1), 180214. https://doi.org/10.1038/sdata.2018.214

Becker, A., Finger, P., Meyer-Christoffer, A., Rudolf, B., Schamm, K., Schneider, U., & Ziese, M. (2013). A description of the global land-surface precipitation data products of the Global Precipitation Climatology Centre with sample applications including centennial (trend) analysis from 1901-present. *Earth System Science Data*, *5*(1), 71–99. https://doi.org/10.5194/essd-5-71-2013

Berghuijs, W. R., Harrigan, S., Molnar, P., Slater, L. J., & Kirchner, J. W. (2019). The relative importance of different flood-generating mechanisms across Europe. *Water Resources Research*, *55*(6), 4582–4593. https://doi.org/10.1029/2019WR024841

Bertola, M., Viglione, A., Lun, D., Hall, J., & Blöschl, G. (2020). Flood trends in Europe: Are changes in small and big floods different? *Hydrology and Earth System Sciences*, *24*(4), 1805–1822. https://doi.org/10.5194/hess-24-1805-2020

CRED & UNDRR. (2020). *Human cost of disasters: An overview of the last 20 years (2000–2019)*. UNDRR. Retrieved from https://www.undrr.org/publication/human-cost-disasters-overview-last-20-years-2000-2019

Do, H. X., Gudmundsson, L., Leonard, M., & Westra, S. (2018a). The Global Streamflow Indices and Metadata Archive (GSIM)-Part 1: The production of a daily streamflow archive and metadata. *Earth System Science Data*, *10*(2), 765–785. https://doi.org/10.5194/essd-10-765-2018

Do, H. X., Gudmundsson, L., Leonard, M., & Westra, S. (2018b). The global streamflow indices and metadata archive-Part 1: Station catalog and catchment boundary [Dataset]. *PANGAEA*. https://doi.org/10.1594/PANGAEA.887477

Do, H. X., Westra, S., & Leonard, M. (2017). A global-scale investigation of trends in annual maximum streamflow. *Journal of Hydrology*, *552*, 28–43. https://doi.org/10.1016/j.jhydrol.2017.06.015

Do, H. X., Zhao, F., Westra, S., Leonard, M., Gudmundsson, L., Boulange, J. E. S., et al. (2020). Historical and future changes in global flood magnitude—Evidence from a model–observation investigation. *Hydrology and Earth System Sciences*, *24*(3), 1543–1564. https://doi.org/10.5194/hess-24-1543-2020

Edokpa, D., Milledge, D., Allott, T., Holden, J., Shuttleworth, E., Kay, M., et al. (2022). Rainfall intensity and catchment size control storm runoff in a gullied blanket peatland. *Journal of Hydrology*, *609*, 127688. https://doi.org/10.1016/j.jhydrol.2022.127688

Fan, Y., & Van Den Dool, H. (2008). A global monthly land surface air temperature analysis for 1948-present. *Journal of Geophysical Research*, *113*(D1), D01103. https://doi.org/10.1029/2007JD008470

Gudmundsson, L., Do, H. X., Leonard, M., & Westra, S. (2018a). The global streamflow indices and metadata archive (GSIM)-Part 2: Quality control, time-series indices and homogeneity assessment. *Earth System Science Data*, *10*(2), 787–804. https://doi.org/10.5194/essd-10-787-2018

Gudmundsson, L., Do, H. X., Leonard, M., & Westra, S. (2018b). The global streamflow indices and metadata archive (GSIM)-Part 2: Time series indices and homogeneity assessment [Dataset]. *PANGAEA*. https://doi.org/10.1594/PANGAEA.887470

Hodgkins, G. A., Dudley, R. W., Archfield, S. A., & Renard, B. (2019). Effects of climate, regulation, and urbanization on historical flood trends in the United States. *Journal of Hydrology*, *573*, 697–709. https://doi.org/10.1016/j.jhydrol.2019.03.102

IPCC. (2021). Climate change 2021: The physical science basis. In *Contribution of working group I to the sixth assessment report of the intergovernmental panel on climate change*. Cambridge University Press. https://doi.org/10.1017/9781009157896

Jiang, S., Bevacqua, E., & Zscheischler, J. (2022). River flooding mechanisms and their changes in Europe revealed by explainable machine learning. *Hydrology and Earth System Sciences*, *26*(24), 6339–6359. https://doi.org/10.5194/hess-26-6339-2022

Kemter, M., Merz, B., Marwan, N., Vorogushyn, S., & Blöschl, G. (2020). Joint trends in flood magnitudes and spatial extents across Europe. *Geophysical Research Letters*, *47*(7), e2020GL087464. https://doi.org/10.1029/2020GL087464

Kim, H., & Villarini, G. (2023a). On the attribution of annual maximum discharge across the conterminous United States. *Advances in Water Resources*, *171*, 104360. https://doi.org/10.1016/j.advwatres.2022.104360

Kim, H., & Villarini, G. (2023b). On the potential use of weather types to describe the interannual variability of annual maximum discharge across the conterminous United States. *Hydrological Processes*, *37*(11), e15014. https://doi.org/10.1002/hyp.15014

Kim, H., & Villarini, G. (2024). Higher emissions scenarios lead to more extreme flooding in the United States. *Nature Communications*, *15*(1), 237. https://doi.org/10.1038/s41467-023-44415-4

Konrad, C. P. (2016). *Effects of Urban development on floods*. U.S. Geological Survey Fact Sheet 076-03. Retrieved from https://pubs.usgs.gov/fs/fs07603/

Lee, J.-Y., Marotzke, J., Bala, G., Cao, L., Corti, S., Dunne, J. P., et al. (2021). Future global climate: Scenario-based projections and near-term information. In V. Masson-Delmotte, P. Zhai, A. Pirani, S. L. Connors, C. Péan, S. Berger, et al. (Eds.), *Climate change 2021: The physical science basis. Contribution of working group I to the sixth assessment report of the intergovernmental panel on climate change* (pp. 553–672). Cambridge University Press. https://doi.org/10.1017/9781009157896.006

Liu, J., Feng, S., Gu, X., Zhang, Y., Beck, H. E., Zhang, J., & Yan, S. (2022). Global changes in floods and their drivers. *Journal of Hydrology*, *614*(PB), 128553. https://doi.org/10.1016/j.jhydrol.2022.128553

Liu, L., Zhang, X., Zhao, T., Gao, Y., Chen, X., & Mi, J. (2021). GISD30: Global 30-m impervious surface dynamic dataset from 1985 to 2020 using time-series landsat imagery on the google Earth engine platform [Dataset]. *Zenodo*. https://doi.org/10.5281/zenodo.5220816

Mallakpour, I., Sadegh, M., & AghaKouchak, A. (2018). A new normal for streamflow in California in a warming climate: Wetter wet seasons and drier dry seasons. *Journal of Hydrology*, *567*, 203–211. https://doi.org/10.1016/j.jhydrol.2018.10.023

Merz, B., Basso, S., Fischer, S., Lun, D., Blöschl, G., Merz, R., et al. (2022). Understanding heavy tails of flood peak distributions. *Water Resources Research*, *58*(6), e2021WR030506. https://doi.org/10.1029/2021WR030506

Merz, B., Blöschl, G., Vorogushyn, S., Dottori, F., Aerts, J. C. J. H., Bates, P., et al. (2021). Causes, impacts and patterns of disastrous river floods. *Nature Reviews Earth & Environment*, *2*(9), 592–609. https://doi.org/10.1038/s43017-021-00195-3

Miniussi, A., Marani, M., & Villarini, G. (2020). Metastatistical extreme value distribution applied to floods across the continental United States. *Advances in Water Resources*, *136*, 103498. https://doi.org/10.1016/j.advwatres.2019.103498

Prosdocimi, I., Kjeldsen, T. R., & Miller, J. D. (2015). Detection and attribution of urbanization effect on flood extremes using nonstationary flood-frequency models. *Water Resources Research*, *51*(6), 4244–4262. https://doi.org/10.1002/2015WR017065

Quintero, F., Villarini, G., Prein, A. F., Zhang, W., & Krajewski, W. F. (2022). Discharge and floods projected to increase more than precipitation extremes. *Hydrological Processes*, *36*(11), e14738. https://doi.org/10.1002/hyp.14738

Rigby, R. A., & Stasinopoulos, D. M. (2005). Generalized additive models for location, scale and Shape. *Journal of the Royal Statistical Society Series C: Applied Statistics*, *54*(3), 507–554. https://doi.org/10.1111/j.1467-9876.2005.00510.x

Schlef, K. E., François, B., Robertson, A. W., & Brown, C. (2018). A general methodology for climate-informed approaches to long-term flood projection—Illustrated with the Ohio river basin. *Water Resources Research*, *54*(11), 9321–9341. https://doi.org/10.1029/2018WR023209

Schneider, U., Becker, A., Finger, P., Rustemeier, E., & Ziese, M. (2020). GPCC Full data monthly Product version 2020 at 0.25°: Monthly land-surface precipitation from rain-gauges built on GTS-based and historical data. https://doi.org/10.5676/DWD_GPCC/FD_M_V2020_025

Schwarz, G. (1978). Estimating the dimension of a model. *Annals of Statistics*, *6*(2), 461–464. https://doi.org/10.1214/aos/1176344136

Slater, L., Villarini, G., Archfield, S., Faulkner, D., Lamb, R., Khouakhi, A., & Yin, J. (2021). Global changes in 20-year, 50-year, and 100-year river floods. *Geophysical Research Letters*, *48*(6), e2020GL091824. https://doi.org/10.1029/2020GL091824

Stein, L., Clark, M. P., Knoben, W. J. M., Pianosi, F., & Woods, R. A. (2021). How do climate and catchment attributes influence flood generating processes? A large-sample study for 671 catchments across the contiguous USA. *Water Resources Research*, *57*(4), e2020WR028300. https://doi.org/10.1029/2020WR028300

Tarasova, L., Lun, D., Merz, R., Blöschl, G., Basso, S., Bertola, M., et al. (2023). Shifts in flood generation processes exacerbate regional flood anomalies in Europe. *Communications Earth & Environment*, *4*(1), 49. https://doi.org/10.1038/s43247-023-00714-8

Trabucco, A., & Zomer, R. (2019). Global aridity Index and potential evapotranspiration (ET0) database: Version 3 [Dataset]. *figshare*. https://doi.org/10.6084/m9.figshare.7504448.v5

Tramblay, Y., & Rouché, N. (2020). ADHI: African database of hydrometric indices [Dataset]. *DataSuds*. https://doi.org/10.23708/LXGXQ9

Tramblay, Y., Rouché, N., Paturel, J.-E., Mahé, G., Boyer, J.-F., Amoussou, E., et al. (2021). ADHI: The African database of hydrometric indices (1950–2018). *Earth System Science Data*, *13*(4), 1547–1560. https://doi.org/10.5194/essd-13-1547-2021

Tramblay, Y., Villarini, G., Saidi, M. E., Massari, C., & Stein, L. (2022). Classification of flood-generating processes in Africa. *Scientific Reports*, *12*(1), 18920. https://doi.org/10.1038/s41598-022-23725-5

UNEP. (1997). World Atlas of desertification (2nd ed.). Retrieved from https://wedocs.unep.org/20.500.11822/30300

Villarini, G., & Wasko, C. (2021). Humans, climate and streamflow. *Nature Climate Change*, *11*(9), 725–726. https://doi.org/10.1038/s41558-021-01137-z

Wasko, C., Nathan, R., & Peel, M. C. (2020a). Changes in antecedent soil moisture modulate flood seasonality in a changing climate. *Water Resources Research*, *56*(3), e2019WR026300. https://doi.org/10.1029/2019WR026300

Wasko, C., Nathan, R., & Peel, M. C. (2020b). Trends in global flood and streamflow timing based on local water year. *Water Resources Research*, *56*(8), e2020WR027233. https://doi.org/10.1029/2020WR027233

Wasko, C., Nathan, R., Stein, L., & O'Shea, D. (2021). Evidence of shorter more extreme rainfalls and increased flood variability under climate change. *Journal of Hydrology*, *603*, 126994. https://doi.org/10.1016/j.jhydrol.2021.126994

Wasko, C., Sharma, A., & Pui, A. (2021). Linking temperature to catastrophe damages from hydrologic and meteorological extremes. *Journal of Hydrology*, *602*, 126731. https://doi.org/10.1016/j.jhydrol.2021.126731

Welty, J., & Zeng, X. (2021). Characteristics and causes of extreme snowmelt over the conterminous United States. *Bulletin of the American Meteorological Society*, *102*(8), E1526–E1542. https://doi.org/10.1175/BAMS-D-20-0182.1

Yao, C., Qian, W., Yang, S., & Lin, Z. (2010). Regional features of precipitation over Asia and summer extreme precipitation over Southeast Asia and their associations with atmospheric–oceanic conditions. *Meteorology and Atmospheric Physics*, *106*(1), 57–73. https://doi.org/10.1007/s00703-009-0052-5

Zhang, S., Zhou, L., Zhang, L., Yang, Y., Wei, Z., Zhou, S., et al. (2022). Reconciling disagreement on global river flood changes in a warming climate. *Nature Climate Change*, *12*(12), 1160–1167. https://doi.org/10.1038/s41558-022-01539-7

Zhang, X., Liu, L., Zhao, T., Gao, Y., Chen, X., & Mi, J. (2022). GISD30: Global 30 m impervious-surface dynamic dataset from 1985 to 2020 using time-series landsat imagery on the Google Earth engine platform. *Earth System Science Data*, *14*(4), 1831–1856. https://doi.org/10.5194/essd-14-1831-2022

Zhang, Y., Zheng, H., Zhang, X., Leung, L. R., Liu, C., Zheng, C., et al. (2023). Future global streamflow declines are probably more severe than previously estimated. *Nature Water*, *1*(3), 261–271. https://doi.org/10.1038/s44221-023-00030-7

Zomer, R. J., Xu, J., & Trabucco, A. (2022). Version 3 of the global aridity Index and potential evapotranspiration database. *Scientific Data*, *9*(1), 409. https://doi.org/10.1038/s41597-022-01493-1